

Exploiting Invariance in Training Deep Neural Networks

Chengxi Ye

Xiong Zhou

Tristan McKinney

Fedor Zhdanov

Amazon Web Services

Yanfeng Liu

Qinggang Zhou

chengxye, xiongzhou, tristamc, liuyanfe, qingganz, fedor@amazon.com

Abstract

Inspired by two basic mechanisms in animal visual systems, we introduce a feature transform technique that imposes invariance properties in the training of deep neural networks. The resulting algorithm requires less parameter tuning, trains well with an initial learning rate 1.0, and easily generalizes to different tasks. We enforce scale invariance with local statistics in the data to align similar samples generated in diverse situations. To accelerate convergence, we enforce a $GL(n)$ -invariance property with global statistics extracted from a batch that the gradient descent solution should remain invariant under basis change. Tested on ImageNet, MS COCO, and Cityscapes datasets, our proposed technique requires fewer iterations to train, surpasses all baselines by a large margin, seamlessly works on both small and large batch size training, and applies to different computer vision tasks of image classification, object detection, and semantic segmentation.

1. Introduction

The pupillary light reflex constricts the pupil in bright light and dilates the pupil in dim light [6]. This mechanism controls the amount of light passing into the eye, allowing common features to be extracted from signals of different scales. In addition, retinal receptive fields use center-surround structures to filter and sharpen images [19] (Supp. Fig. 5 a, b), removing a bell-shaped autocorrelation present in real-world visual signals. Fascinatingly, all other receptive field configurations discovered in Hubel and Wiesel's seminal research (Supp. Fig. 5 c, d, e) have found artificial analogs in the first layer filters learned by modern convolutional neural networks [46] (Fig. 5 a,b).

While convolutional networks continue to push the envelope in computer vision tasks, state-of-the-art training recipes are still limited by scope and scale. Specifically, when moving from image classification to object detection, different normalization techniques need to be used. Most algorithms perform well at a specific scale, and there is usu-

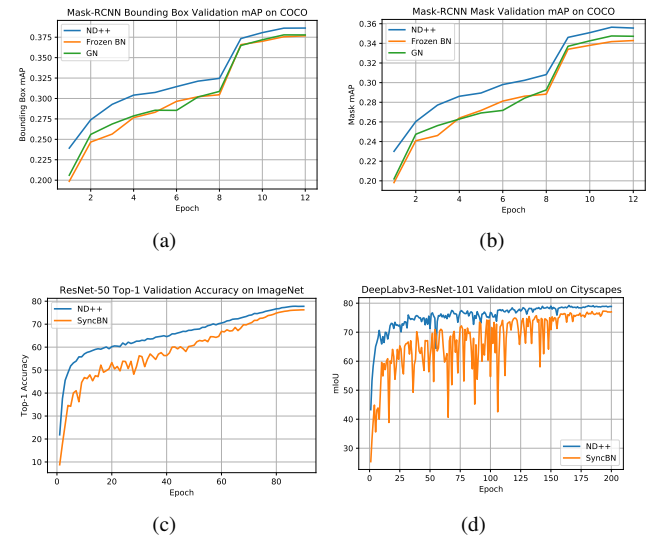


Figure 1. (a,b) Validation AP curves of a Mask R-CNN network when trained with network deconvolution++ (ND++), frozen batch normalization and group normalization. (c) Top-1 validation accuracy of ResNet-50 when trained on ImageNet with ND++ and SyncBN using batch size of 2048, the training finishes better and faster than using batch size 256 using the same hardware. (d) mIoU curves of DeepLabv3 with a ResNet-101 backbone trained on the Cityscapes dataset using ND++ and SyncBN. ND++ consistently outperforms baselines and produces more stable mIoU curves.

ally a significant drop in accuracy when the training batch size is too large or too small [39, 34].

In this paper, we conduct a study of a one-layer linear network to understand the origin of these limitations. Drawing inspiration from this study, the structure of animal visual systems, and recent related work [41], we derive two invariance properties that enhance the training of deep neural networks. We implement cross-GPU synchronization to aggregate the computation required to enforce the invariance, surpassing the widely used synchronized batch normalization [31] method significantly. This implementation allows us to support both small batch and large batch

training without algorithm change. By enforcing the invariance properties at every layer of the network, we accelerate training convergence and surpass baseline accuracy by a large margin on the ImageNet [9], MS COCO [26], and Cityscapes [8] datasets for image classification, object detection, and semantic segmentation, respectively (Fig. 1). In our supplementary materials, we also show promising results on multiple language tasks.

Our contributions are the following:

- We provide a novel analysis of neural network training techniques and show that enforcing certain invariance properties improve the optimality of the training.
- We propose a drop-in modification *before* the linear layers in the network to explicitly enforce these invariance properties. With the proposed modification, algorithms require fewer iterations to train and surpass baseline accuracy by a large margin.
- We implement a cross-GPU synchronization for our approach and show it surpass synchronized batch normalization by a large margin in the small batch regime.
- Our method generalizes to the large batch regime without ad hoc tuning, increasing the training throughput without a significant drop in accuracy.
- Training with the modification is robust to different optimizer configurations; using the theoretically optimal learning rate for the linear case of 1.0 can successfully train a wide range of deep networks.
- The benefits of the proposed modification are demonstrated for computer vision tasks such as image classification, object recognition, semantic segmentation and several language tasks over multiple major datasets and architectures.

2. Background

2.1. Backward Correction Methods

The complicated loss landscapes [25] of neural networks create numerous challenges for training. Deep neural networks are generally over-parameterized. The presence of strong correlation between features induces areas of pathological curvature in the landscape and inhibits effective training. Small gradients are common in these pathological regions, and the problem is exacerbated by small linear layers and common activation functions. These issues were traditionally addressed by correcting the gradients [29, 27, 43], that is, by modifying the backward pass. The most popular methods normalize the gradient scale to avoid the vanishing gradient problem and smooth the direction by using previous gradients as a momentum term [22]. More advanced

methods use approximate curvature information to maneuver the gradient direction (Fig. 2). However, high computational costs limit these algorithms to small-scale problems [28, 10]. They have not been widely shown to surpass first-order gradient descent methods.

2.2. Forward Correction Methods

Forward transforms provide an alternative approach to address the challenges in training deep neural networks [16]. Batch normalization [21] is a common and powerful example that standardizes the distribution of features in each dimension. This stretching with a diagonal matrix works perfectly only for uncorrelated, axis-aligned features, suggesting that the optimality of standardization *depends on the choice of basis*. Given the inherent correlation in real-world data, the feature covariance matrix is generally ill-conditioned and not diagonal. As a result, gradient descent training usually takes unnecessary steps towards the solution (Fig. 2(b)). Recently, more accurate transforms have been proposed to utilize the covariance matrix and remove the pairwise correlation between features [17, 42, 18, 30, 41]. If the features are transformed to be axis-aligned and have unit-variance, the loss landscape is more isotropic. Gradient descent converges more quickly and accurately (Fig. 2(c)).

2.3. Small and Large Batch Training of Neural Networks

Various techniques have been proposed to extend the scale of deep neural network training. Since batch normalization was empirically found to perform well at a medium to large scale, follow-up techniques have been proposed to normalize each sample [39, 5, 34] or model weight [33, 32] to support the small sample scenario.

As modern GPUs can handle increasingly large batch sizes, accelerating the training convergence has become an important topic. In the large scale setting, the standard rule of thumb is that the learning rate should scale linearly with the batch size [23]. Unfortunately, the increased learning rate requires careful compensatory tuning, and training can easily explode or end with degraded results. Ad hoc techniques such as warmup and layerwise learning rate adaptation [45] are widely utilized on multiple tasks [12, 14, 31, 38]. To date, there is no clear theoretical justification for these approaches and it is not clear how well these approaches generalize to other scenarios.

3. Motivations

We start our investigation with a toy example of a one-layer network (Eq. 1). Rigorous analysis of this simple setup reveals a surprising depth of insight into the fundamental training problem. The analysis explains the utility

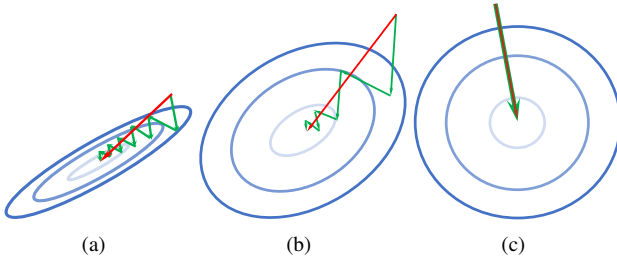


Figure 2. A toy picture of loss landscapes corresponding to (a) highly correlated, non-standardized data, (b) correlated but standardized data, and (c) standardized and uncorrelated data. The red arrows correspond to the gradients found through backward correction methods and the green arrows correspond to the gradients used in gradient descent iterations.

of various modern techniques to facilitate training and leads us to the more advantageous design we propose.

Assume we are given a linear regression problem with mean squared error (Eq. 1). \hat{y} is the continuous or discrete response data to be regressed. This formulation can be used for prediction or classification. In a typical setting, the output $y = Xw$ is given by multiplying the inputs X with an unknown weight vector w , which we are solving for. Let N be the number of samples and d be the feature dimension, then X can be the $N \times d$ data matrix or the augmented $N \times (d + 1)$ data matrix ($X|\mathbf{1}$) if we consider the bias.

$$Loss_{MSE} = \frac{1}{2} E(|y - \hat{y}|^2) = \frac{1}{2N} \|Xw - \hat{y}\|^2. \quad (1)$$

3.1. Local Statistics vs Global Statistics

Given a $N \times d$ data matrix X , we refer to the column statistics as the *global statistics* and the row statistics as *local statistics*. Mini-batch statistics represent an approximation to the global statistics of the whole dataset. Batch normalization [21] standardizes the d column vectors. This can be visualized as a coordinate transform that stretches the data along each axis based on global statistics (Fig. 2 (a) to (b)). Training then solves for a *new set of weights* w_{BN} in this transformed space.

On the other hand, sample-based normalization [5, 39, 34] stretches each sample by removing the scale and bias in each row of X according to the local statistics. Viewed from the original space, training corresponds to finding N sets of *sample-variant weights* $\{w_i\}$ that both stretch the samples and fit the model.

3.2. $GL(n)$ -invariance

One may ask whether the solution of Eq. 1 found using a given algorithm changes under a change of basis. That is, if we use any invertible linear transform, known as the general linear group $GL(n)$ [4], to transform the features, will

we simply reach an equivalent solution in a different coordinate system? If the solution is invariant under the operation of $GL(n)$, we will call the training algorithm $GL(n)$ -invariant.

Assuming $X^t X$ is invertible for our toy problem, the unique solution can be found by setting the gradient to 0, $\frac{\partial Loss}{\partial w} = \frac{1}{N} X^t (Xw - \hat{y}) = 0$,

$$w = (X^t X)^{-1} X^t \hat{y}. \quad (2)$$

Let us consider the impact of different correction methods on the ability of gradient descent-based algorithms to find this solution.

Case 1 (backward correction): For simplicity, suppose we start from $w_0 = 0$, then $\frac{\partial Loss}{\partial w}|_{w_0} = -\frac{1}{N} X^t \hat{y}$. Letting $H = \frac{1}{N} X^t X = \nabla^2 w$, we see from Eq. 2 that $w = -H^{-1} \frac{\partial Loss}{\partial w}$. This derivation shows us how the gradients can be manipulated in the backward fashion to accelerate convergence [28, 10, 43]: (1) approximate the curvature with H and apply an inverse correction to *decorrelate the gradient*, $H^{-1} \frac{\partial Loss}{\partial w}$, then (2) take a descent step using a learning rate of 1.0: $w = w_0 - 1.0 \cdot H^{-1} \frac{\partial Loss}{\partial w}$. $GL(n)$ invariance can be achieved because the optimal solution can be found in one step by following the corrected negative gradient in *any basis* (found as the red arrows in Fig. 2).

Case 2 (forward correction): From the forward correction point of view, standardization using global statistics results in standardized columns, while using local statistics results in standardized rows. In terms of convergence rate, using global statistics is slightly superior, as after correction $\frac{1}{N} H = \frac{1}{N} X^t X$ is guaranteed to have unit diagonal. Therefore, the loss landscape has better statistical properties and convergence is accelerated.¹ However, standardization with either local or global statistics does not remove correlations between features. On an elongated energy landscape, gradient descent algorithms generally do not converge in one step and the optimal solution cannot be found under an arbitrary basis change.

In fact, the optimal solution can be found in one step with the forward correction if and only if the feature *columns* are standardized and uncorrelated. With these features we have $\frac{1}{N} X^t X = I$, and the optimal explicit solution (Eq. 2) simplifies to $w = \frac{1}{N} X^t \hat{y}$. After one iteration of gradient descent, $w_{new} = w_{old} - \eta \frac{1}{N} (X^t X w_{old} - X^t \hat{y})$. By substituting $\frac{1}{N} X^t X = I$, we find that $\eta = 1.0$ is optimal and yields convergence in a single iteration. This demonstrates that if we (1) *decorrelate the feature columns with global statistics* and (2) use a learning rate 1.0, forward correction can be modified to be $GL(n)$ -invariant and achieve optimal convergence.

¹Normalization with local statistics works on XX^t , which is less related to the convergence.

3.3. Scale Invariance

In our toy problem, the output scales linearly with the input, $(aX)w = a(Xw)$. This property actually generalizes to common networks with linear layers and ReLU-like activation functions; one only needs to replace w with the composite transform matrix W to see this. If we consider a task like bounding box prediction, this suggests that we can scale the box size by simply changing the input brightness, which should clearly be avoided. Through pupillary light reflex, animal visual systems introduce a scale invariance property so that different scaled inputs generate similar scaled features. Although transform using global statistics can guarantee $GL(n)$ -invariance as discussed above, it does not give us the scale invariance property. When scale invariance is a concern in some tasks, local statistics may be considered to transform the samples individually. This motivates us that two sets of statistics should be involved in the algorithm and we defer the explanation of our design detail to the next section.

3.4. Optimizing the Formulation

Influenced by the batch normalization, most normalization algorithms [5, 39, 34, 17, 17, 18, 30] empirically adopt a post-normalization design, normalizing after the linear transform, on $y = Xw$ rather than on X . Since post-normalization restricts the representation power of y , two extra parameters are introduced to remove this limitation: $Loss_{MSE} = \frac{1}{2N} \|(Xw - \mu)\Sigma^{-1}\gamma + \beta - \hat{y}\|^2$. As a result, the toy problem contains more than necessary parameters (w, γ, β instead of w) to be optimized. The redundancy is also common in weight normalization techniques [32, 15]. In this direction, constraints such as unit norm or orthonormality have been enforced on w . Without the extra parameters, the constraints also prevent us from getting the optimal solution. However, the optimal convergence property that we find on the toy problem no longer holds with the introduction of the redundancy. This motivates us to optimize our design to remove the redundancy while maintaining full representation power.

3.5. Simplifying Training

Though deep neural networks contain nonlinearities, gradient descent training is based on a local linear approximation. We suspect an optimal training method should still have these optimal properties of training with uncorrelated features and using learning rate 1.0. However, neither of them is common in the present state-of-the-art. Popular optimizers [22] usually have small default learning rates, such as 0.001. As modern hardware can handle more and more data, the linear scaling rule recommends that the learning rate should scale linearly with the batch size. As a result, > 10.0 learning rates can be found in large batch experiments [12]. These recipes require heavy tuning, and it is

common to see warmup, task-specific optimizers, and lay-
erwise learning rate adaptation [45] to avoid gradient ex-
plosion [14, 31, 38]. The large learning rate creates a se-
vere obstacle when the training scale or task is changed. By
following the principles suggested in the toy problem, we
demonstrate that a fixed learning rate can be used to benefit
from the increasingly more powerful hardware.

4. Enforcing Invariance in Training Neural Networks

In this section, we demonstrate how the problems in the previous section can be naturally resolved. Some complementary information can be found in recent works [41].

To improve the network training, we enhance the linear transform in neural networks by applying the principles de-
rived from the toy problem. We discuss how to enhance
three common linear transform layers, starting from ana-
lyzing the data matrice X in the network.

Case 1. The data matrix X of a fully-connected layer is
constructed straightforwardly by stacking N rows of d or
 $d + 1$ dimensional feature vectors. We put our emphasis
on the data matrix construction of convolution and (cross-)
correlation layers.

Case 2. A convolution operation can be expressed in
multiple ways in the spatial domain. We can expand the
kernel of size k into a $(n - k + 1) \times n$ convolution matrix W ,
or unroll the overlapping windows of x into a $(n - k + 1) \times k$
data matrix X : $y = x * w = Wx = Xw_{flipped}$. We provide
a 1d convolution example using $k = 3$ (in the ‘valid’ mode
according to Matlab terminology):

$$\begin{pmatrix} y_1 \\ y_2 \\ \dots \\ y_{n-k} \\ y_{n-k+1} \end{pmatrix} = \begin{pmatrix} w_3 & w_2 & w_1 & & & \\ & w_3 & w_2 & w_1 & & \\ & & \ddots & & & \\ & & & w_3 & w_2 & w_1 \end{pmatrix} \begin{pmatrix} x_1 \\ x_2 \\ \dots \\ x_{n-1} \\ x_n \end{pmatrix}$$

$$= \begin{pmatrix} x_1 & x_2 & x_3 \\ x_2 & x_3 & x_4 \\ x_3 & x_4 & x_5 \\ \dots & & \\ x_{n-3} & x_{n-2} & x_{n-1} \\ x_{n-2} & x_{n-1} & x_n \end{pmatrix} \begin{pmatrix} w_3 \\ w_2 \\ w_1 \end{pmatrix}$$

Case 3. The correlation operation (also called trans-
posed convolution, or sometimes misnamed as deconvolu-
tion) is the adjoint operation of the convolution, and in-
volves padding the data by $k - 1$ on each side (correspond-
ing to the ‘full’ mode in Matlab terminology) and using the
unflipped kernel. The data matrix of correlation only dif-
fers from that in the convolution by the zero padding and is

omitted here.

$$\begin{pmatrix} y_1 \\ y_2 \\ \dots \\ y_{n-1} \\ y_n \end{pmatrix} = \begin{pmatrix} w_1 & w_2 & w_3 & & & \\ & w_1 & w_2 & w_3 & & \\ & & \ddots & & & \\ & & & w_1 & w_2 & w_3 \end{pmatrix} \begin{pmatrix} 0 \\ 0 \\ x_1 \\ x_2 \\ \dots \\ x_{n-k+1} \\ 0 \\ 0 \end{pmatrix}$$

By closely looking at the different columns in the convolution/correlation data matrix X (in case 2), one can find a rarely discussed problem in the training of networks. Since real-world data exhibits strong autocorrelation, and the neighboring columns of the data matrix correspond to shifting the signal by one pixel, the feature dimensions in the convolution/correlation data matrices are *heavily correlated*. Therefore gradient descent training cannot converge efficiently with existing standardization techniques (Fig. 2 (b)) or just by decorrelating the feature channels in a layer.

In signal processing, removing such pixel-wise autocorrelation has a long history and can be achieved through a process called whitening deconvolution [11]. This correlation removal process can be generalized to every layer of a convolution neural network and we call this procedure network deconvolution. Usually this is achieved in the frequency domain through spectral whitening, i.e. a normalization in the frequency domain: $\frac{\mathcal{F}(x)}{|\mathcal{F}(x)|} = \frac{\mathcal{F}(x)}{\sqrt{\mathcal{F}^H(x) \cdot \mathcal{F}(x)}}$. This elegant normalization shows a profound insight: the optimal standardization for the convolution operation should in fact be carried out in the frequency domain. Note that frequency multiplication corresponds to a spatial domain convolution, and the frequency division corresponds to a spatial domain *deconvolution*. Moreover, the deconvolution kernel $\mathcal{F}^{-1}(\frac{1}{|\mathcal{F}(x)|})$ has been found to resemble the center-surround structures in animal visual systems (Supp. Fig. 5(a,b)) [19, 20, 41]. Four lines of Matlab code are provided here for a quick verification (Fig. 3).

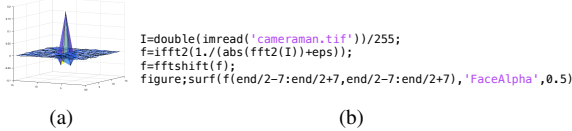


Figure 3. Visualizing a frequency domain deconvolution filter in the spatial domain leads to a structure that has positive center values and negative surround values, resembling an on-center cell in animal visual systems [19] (Supp. Fig. 5(a)).

For convolutional neural networks, the deconvolution computation should better be carried out in the spatial domain using the data matrix X to match the small kernels that are used in practice. Specifically we calculate the co-

variance matrix $Cov = \frac{1}{N}X^tX$, find its unique principal inverse square root: $D = Cov^{-\frac{1}{2}}$, then use this matrix to transform the data matrix: $X_0 = X \cdot D$. Note that $\frac{1}{N}X_0^tX_0 = Cov^{-\frac{1}{2}} \cdot Cov \cdot Cov^{-\frac{1}{2}} = I$. As the transformed features are uncorrelated and standardized, a faster convergence is achieved in this corrected space (Fig. 2(c)). The gradient found in this uncorrelated new space can be transformed back uniquely to find the gradient in the original non-axis-aligned space, therefore $GL(n)$ -invariance is achieved. During the training, we keep track of the correction D , and use the running average during testing.

For a convolution/correlation layer with C channels, we construct the data matrix for each channel then horizontally concatenate the C data matrices into a wider matrix (with Ck/Ck^2 columns for $1d/2d$). Deconvolution with this wider matrix removes the correlation of k/k^2 *nearby pixels* and C *feature channels* at once (see Supp. Sec. B).

Experiments show that the above formulation works well for simple classification tasks that do not require scale invariance (see results in Sec. 6.5). However, it may not work well for some other tasks such as object detection and instance segmentation, in which scale invariance plays an important role. To generalize the benefits of network deconvolution to these tasks, we incorporate local statistics to remove the scale in each individual sample. This simple strategy is inspired by the biological observation that *animal visual systems also use two sets of statistics for visual analysis* [19, 6]. The retinal light reflex [6] suggests local statistics is used to adjust the scale of the signal. For a fully-connected layer, the local statistics is calculated from each row of the data matrix X . For a convolution/correlation layer, the local statistics can be either calculated for one or more rows of the data matrix, or even for the feature tensor at each layer. In our development, we have found the latter option works well and does not introduce an excessive computational cost. At each layer we standardize each sample tensor interchangeably with μ, σ [5], or with mean l_1 norm $E(|x|)$ if we just consider the scale. Combined with the linear transform weights, our proposed feature transform is:

$$y = S \cdot X \cdot D \cdot w. \quad (3)$$

Here S is the standardization operating on the *rows* of X , which is a diagonal matrix ($\frac{1}{\sigma_i}$) if we only consider the scaling or augmented by an extra column ($-\frac{\mu_i}{\sigma_i}$) if we also consider the bias. And D is the decorrelation operating on the *columns* of $S \cdot X$. Weight is trained in the transformed space, based on the uncorrelated features $S \cdot X \cdot D$.

Our formulation transforms both the rows and columns of X , with no redundancy introduced. Normalization using local statistics enforces scale invariance, aligning features of different scales. Normalization with global statistics enforces $GL(n)$ -invariance, leading to faster convergence.

5. Implementation Details

5.1. Cross-GPU Synchronization

To embrace the advancements in the latest hardware development, we implement cross-GPU synchronization to improve the quality of the estimates ². At each layer, the covariance matrix is computed on each GPU and synchronized across all the GPUs. On an 8-GPU machine, the synchronization cost is negligible. This implementation allows us to collect reliable statistics throughout the training for all practical batch sizes. In our development, we have consistently achieved satisfactory results using per-GPU batch sizes from 2 to 1024 under 8-GPU training environment without much tuning.

5.2. Acceleration Techniques

Even though the complexity of the proposed algorithm is usually a small fraction of the cost of a convolution layer (Supp. Table 8), current deep learning libraries do not support efficient computation of the covariance matrix. The memory accessing time of extracting the data matrix from a convolution/correlation layer takes significantly more time than the underlying convolution operation in PyTorch. We discuss some of our implementation details for all the experiments, and leave the complexity derivation in the supplementary material (Supp. Sec. C). We adopt a $3 \times$ -subsampling for ImageNet scaled images and $5 \times$ -subsampling for MS COCO scaled images. The data and covariance matrices are computed using tensor patches sampled at the strided locations, reducing the construction cost by $9 \times$ and $25 \times$ respectively. Since the involved number of pixels is usually more than enough, we notice this strategy maintains accuracy while keeping the computational footprint low. When the covariance matrix becomes too large, we divide the columns into blocks and decorrelate between the blocks [43, 17]. In our experiments, we set the number of blocks $B = 256$ for fully-connected layers and $B = 64 \times k^2$ for convolution/correlation layers.

There are multiple ways [17, 42, 18, 41] to calculate the principal inverse square root of a matrix but algorithms that are both efficient and stable are scarce. Since explicit eigenvalue decomposition is slow, Newton Schultz iteration becomes a faster alternative. However, vanilla Newton Schultz method is unstable under finite arithmetic [41] (Fig. 7), here we adopt a coupled inverse Newton iteration method that is numerically stable and works well under finite precision arithmetic [13]. Starting with $X_0 = I$, $M_0 = Cov$, the coupled inverse Newton iteration calculates $X_{k+1} = X_k \frac{(3I - M_k)}{2}$, $M_{k+1} = \left(\frac{(3I - M_k)}{2}\right)^2 M_k$ and produces $X_k \rightarrow Cov^{-\frac{1}{2}}$. Empirically, using 5 iterations yields good results.

²An independent implementation can also be found [30].

Note that the forward correction is equivalent to the backward correction if we only consider one layer. However, the covariance matrix in a deeper layer relies on the variables in a shallower layer. While this functional relation can be natively captured in the forward fashion with the help of automatic differentiation libraries, it cannot be easily captured by existing backward correction methods. In our development, we have simulated the backward correction methods by excluding inverse square root calculations from the gradient descent training but noticed a moderate accuracy drop. This observation suggests that the inclusion of the covariance matrix related computation in the computational graph can promote more optimal gradients throughout the network.

We also add a small diagonal matrix ϵI to the covariance matrix to avoid rank-deficiency. Note that an attractive idea is to include the population statistics, i.e., the running average of the covariance, for stabilization [44, 40]. We have tried but do not pursue this option due to an inherent limitation that the smoothing factor needs to be small to avoid transforming the current batch with a mismatched geometry, leading to a training explosion.

Note that for a large data matrix X , decorrelating columns of X can take excessive computation. Previous applications are usually restricted to a small number of layers [17, 18, 30], which adds to the network design complexity. We adopt a universal design, however, we avoid the excessive computation by reordering the computation. We transform the model weights instead $y = (S \cdot X) \cdot (D \cdot w)$.

6. Experiments

We refer to our improved implementation as Network Deconvolution++ (ND++). ND++ introduces scale invariance, generalizes the $GL(n)$ -invariance to all three common linear transform layers (convolution/correlation/linear) in modern architectures, and uses cross-GPU synchronization to allow reliable training at different scales. In the following experiments, all linear transform layers are enhanced with ND++. The numbers reported in this section are based on the settings described in Sec. 5.2. In fine-tuning experiments, the pretrained backbone network is replaced with a backbone pretrained with ND++. For a fair comparison, we have also experimented with training from scratch to verify the gain is not only from the improved backbone. Standard stochastic gradient descent is used for all experiments. We continue to use learning rate decay in the face of inherent non-linearity and the mini-batch training.

6.1. Image Classification

We demonstrate improved training on three popular CNN architectures (VGG, ResNet, DenseNet) at three scales (10/50/100 layers). With ND++ we have seamlessly increased the training to batch size 2048, eight times

Network	SyncBN	ND++
VGG-11	71.11	72.24
ResNet-50	76.25	77.95
ResNet-101	77.37	79.40
DenseNet-121	74.65	76.11

Table 1. Top-1 Validation Accuracy on the ImageNet Dataset. ND++ also surpasses the top-1 accuracy rates of the deeper networks in the model zoo: VGG-13: 71.55%, ResNet-101: 77.37%, ResNet-152: 78.32%, DenseNet-169: 76.00%.

	MB	MLPerf	Detectron2
ND++	37.36	37.37	39.01
BN	36.78	36.35	37.9
GN	36.04	35.9	38.54

Table 2. Bounding box AP of three Faster R-CNN implementations on the COCO 2017 dataset.

	MB		MLPerf		Detectron2	
	AP ^{bbox}	AP ^{mask}	AP ^{bbox}	AP ^{mask}	AP ^{bbox}	AP ^{mask}
ND++	38.62	35.65	38.36	35.07	39.91	36.87
BN	37.67	34.28	37.14	33.97	38.6	35.2
GN	37.82	34.75	36.32	33.52	38.96	35.93

Table 3. Bounding box and mask AP of three Mask R-CNN implementations on the COCO 2017 dataset.

larger than the model zoo default setting of 256. We train in one-eighth the number of iterations but produce superior models (Table 1). All three network architectures, VGG-11/ResNet-50/ResNet-101/DenseNet-121, surpass *their deeper counterparts* in the model zoo after standard 90-epoch training with cosine learning rate decay. Using the official PyTorch recipe, it takes less than one day to train on a machine with 8 Nvidia A100 GPUs compared to days or even a week with smaller batch sizes. On the popular ResNet-50/101 network, the 77.95%/79.40% top-1 accuracy we reach is among the highest numbers reported when training for 90 epochs (Fig. 1(c)). In the large batch setting, our results improve on previously reported performance reached with careful tuning, e.g., 76.51% [12] using the same batch size, 76.1% [35] by increasing the batch size instead of using learning rate decay, or 77.73% [14] with an improved ResNet-50D model using a smaller batch size of 1024 and training for 120 epochs. We also improve upon recent decorrelation techniques that do not handle pixel-wise correlation (see Supp. Sec. F).

6.2. Object Detection

We test ND++ on Faster R-CNN and Mask R-CNN, milestone object detectors from three major benchmarks, *maskrcnn-benchmark*(MB) [2], *MLPerf* [3], and *Detectron2*. We use ResNet-50 with FPN as backbones and two fully-connected layers in the box heads. In Mask R-CNN, the mask head contains convolution and correlation layers. ND++ is used to enhance all layers. We report our numbers and evaluation curves on the COCO 2017 dataset (Ta-

	LR	AP ^{bbox}	AP ^{mask}
ND++	0.02	37.81	34.87
GN	0.02	37.76	34.8
ND++	0.1	38.86	35.56
GN	0.1	35.21	33.66

Table 4. Mask R-CNN trained from scratch on the COCO 2017 dataset.

Batch	LAMB	MegDet	ND++	
	AP ^{bbox}	AP ^{bbox}	AP ^{bbox}	AP ^{mask}
128	36.7	37.7	38.61	35.54
256	36.7	37.7	38.40	35.26
512	36.5	-	37.45	34.5

Table 5. Large-scale training performance of Mask R-CNN using ND++. Our reported numbers are based on the NVIDIA implementation. ND++ significantly surpasses MegDet [31] and LAMB [38] that utilize SyncBN, warmup and optimizer change.

bles 2, 3, Fig. 1(a,b)). Results with ResNet-101 can be found in Supp. Sec. E.2, Supp. Tab. 9.

On all three benchmarks and with both Faster R-CNN (Table 2) and Mask R-CNN (Table 3), ND++ consistently outperforms baselines with frozen batch normalization and group normalization [39] in terms of Average Precision(AP) (Fig. 1(a,b)). On the more powerful Mask R-CNN architecture, we conduct a comparative study of training from scratch. In the default configuration, the initial learning rate is set to 0.02, the same as for fine-tuning. With this initial learning rate, ND++ consistently outperforms group normalization throughout training. When we increase the learning rate to the more standard 0.1 for training from scratch, group normalization ends up with worse results while ND++ finishes better (Table 4, Supp. Fig. 7).

Though researchers have encountered severe challenges in scaling up the training of Mask R-CNN [31, 38], we have been able to seamlessly increase the batch size and achieve good results without ad hoc techniques. Here we take the MLPerf implementation, remove the warmup stage, and fix the learning rate to 0.1 with a momentum of 0.9. We notice that frozen/synchronized batch normalization explodes at all scales without warmup while ND++ produces superior results. ND++ significantly surpasses the MLPerf accuracy goal³ within the standard 12-epoch fine-tuning with batch sizes up to 256, an order of magnitude larger than most existing baseline settings (Table 5, Supp. Fig. 8). Note that recent large-scale training techniques that utilize synchronized batch normalization may not reach this goal, while ND++ can surpass this goal in the 10/11-th epoch. ND++ is trained for 11250, 5625, and 2813 iterations at batch sizes of 128, 256, and 512, respectively.

Network	SyncBN	ND++
DLv3-RN-50 (scratch, 200 ep.)	69.30	72.69
DLv3-RN-50 (finetune, 200 ep.)	75.70	77.50
DLv3-RN-101 (finetune, 200 ep.)	77.28	79.23
DLv3-RN-50 (finetune, 50 ep.)	-	76.47
DLv3-RN-50 (finetune, 500 ep.)	75.71	-

Table 6. Validation mIoU when fine-tuning and training from scratch on the Cityscapes dataset. DLv3 stands for DeepLabv3 and RN stands for ResNet.

ResNet-50 top-1	Mask R-CNN (MLPerf)		DeepLabv3-RN-50 mIoU (Scratch)
	AP bbox	AP mask	
77.66	38.26	35.41	71.64

Table 7. Experiments with an initial learning rate 1.0 and no momentum.

6.3. Semantic Segmentation

To demonstrate the usefulness of ND++ for semantic segmentation, we add ND++ layers to the DeepLabv3 architecture [7] with both ResNet-50 and ResNet-101 backbones and test the performance on the Cityscapes dataset [8]. We use a base resolution of 1024 for the images. To show that ND++ is consistently useful with different computational resources, we use a minibatch size of 3 images per GPU for the ResNet-50 experiments on NVIDIA V100 GPUs and 8 images per GPU for the ResNet-101 experiments on NVIDIA A100 GPUs. We train for 200 epochs for all experiments unless stated otherwise. We perform fine-tuning experiments with a ResNet-50 backbone pretrained on ImageNet with an initial learning rate of 0.01 and 0.1 and momentum 0.9 for both ND++ and the SyncBN baseline, and we report the results with learning rate 0.01 for SyncBN and 0.1 for ND++ in Table 6 since these produced the best results for each network configuration. Note that the performance of our ResNet-50 model with ND++ is 77.50, comparable to the ResNet-101 model from the original paper with 77.82 mIoU for single-scale evaluation [7].

We find that an initial learning rate of 0.1 and momentum 0.9 produces better performance for all other experiments, including finetuning with a pretrained ResNet-101 backbone and training from scratch with a ResNet-50 backbone (Table 6, Supp. Table. 11). ND++ substantially improves over the synchronized batch norm baseline. And the acceleration is especially apparent early in training. For example, it takes less than 50 epochs for a network equipped with ND++ to beat the performance of a network trained using SyncBN for 500 epochs (Supp. Fig. 10 and Table 6) if we fine-tune using a pretrained ResNet-50 backbone.

6.4. Experiments with Learning Rate 1.0

Existing deep neural network models are trained with stochastic gradient descent algorithm variants with momen-

tum [36]. Although the momentum term usually has a beneficial effect of reducing the noise and accelerating convergence, we notice that with ND++, many networks train well with a initial learning rate 1.0 and without the use of the momentum term, presumably thanks to the $GL(n)$ -invariance property (Table 7).

6.5. Ablation Studies

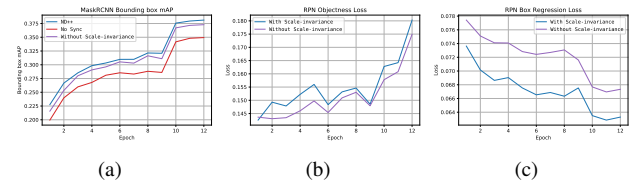


Figure 4. Ablation study on the Mask R-CNN architecture.

Cross-GPU synchronization and scale invariance produce larger improvements in the more advanced two-stage detector Mask R-CNN as indicated by ablation experiments on the MLPerf benchmark (Fig. 4 (a)). To further study the effect of enforcing scale invariance, we separately plot the objectness classification and regression losses for the region proposal network (RPN) (Fig. 4 (b,c)). Without scale invariance, the object classification loss remains lower throughout the training, but the bounding box regression loss is higher. The inaccurate proposals likely pull down the final results (Fig. 4 (a) the purple curve).

Similar to object detection, we find cross-GPU synchronization markedly improves performance (from 69.82% to 72.69%) for semantic segmentation (Supp. Table 11). However, unlike for object detection, enforcing scale invariance has very little effect. Given this fact, we report results without enforcing scale invariance in Table 6 and Fig. 1.

For ImageNet training, the difference is less noticeable, consistent with the findings in the literature [39]. We see a tiny improvement by enforcing scale invariance, while synchronization does not seem to give us a significant gain due to the per GPU batch size of 256. If we remove both synchronization and scale invariance, the top-1 accuracy of ResNet-50 drops slightly to 77.80%.

7. Discussion

The transform we propose has simple and intuitive geometric meanings. To achieve scale invariance, each sample is stretched individually using local statistics. The global geometry of the loss landscape, however, depends on the full collection of data. We therefore utilize the global distribution of data to find a unique optimal feature transform and achieve $GL(n)$ -invariance. The unique gradient direction in the this space corresponds to the optimal direction in the linear case and leads to significantly accelerated training of deep neural networks.

³37.7 for bounding box AP and 33.9 for mask AP.

References

[1] Fairseq. <https://github.com/pytorch/fairseq>. Accessed: 2021-01-01. 13

[2] maskrcnn-benchmark. <https://github.com/facebookresearch/maskrcnn-benchmark>. Accessed: 2021-01-01. 7

[3] Mlperf training v0.7. <https://github.com/NVIDIA/DeepLearningExamples>. Accessed: 2021-01-01. 7

[4] M. Artin. *Algebra*. Pearson Prentice Hall, 2011. 3

[5] Jimmy Lei Ba, Jamie Ryan Kiros, and Geoffrey E. Hinton. Layer normalization, 2016. 2, 3, 4, 5, 11

[6] Mark Bear, Barry Connors, and Michael A Paradiso. *Neuroscience: Exploring the brain*. Jones & Bartlett Learning, LLC, 2020. 1, 5

[7] Liang-Chieh Chen, George Papandreou, Florian Schroff, and Hartwig Adam. Rethinking atrous convolution for semantic image segmentation. *arXiv preprint arXiv:1706.05587*, 2017. 8

[8] Marius Cordts, Mohamed Omran, Sebastian Ramos, Timo Rehfeld, Markus Enzweiler, Rodrigo Benenson, Uwe Franke, Stefan Roth, and Bernt Schiele. The cityscapes dataset for semantic urban scene understanding. In *Proceedings of the IEEE conference on computer vision and pattern recognition*, pages 3213–3223, 2016. 2, 8

[9] Jia Deng, Wei Dong, Richard Socher, Li-Jia Li, Kai Li, and Li Fei-Fei. Imagenet: A large-scale hierarchical image database. In *2009 IEEE conference on computer vision and pattern recognition*, pages 248–255. Ieee, 2009. 2

[10] Guillaume Desjardins, Karen Simonyan, Razvan Pascanu, and koray kavukcuoglu. Natural neural networks. In C. Cortes, N. D. Lawrence, D. D. Lee, M. Sugiyama, and R. Garnett, editors, *Advances in Neural Information Processing Systems 28*, pages 2071–2079. Curran Associates, Inc., 2015. 2, 3

[11] Rafael C. Gonzalez and Richard E. Woods. *Digital Image Processing (3rd Edition)*. Prentice-Hall, Inc., USA, 2006. 5

[12] Priya Goyal, Piotr Dollár, Ross Girshick, Pieter Noordhuis, Lukasz Wesolowski, Aapo Kyrola, Andrew Tulloch, Yangqing Jia, and Kaiming He. Accurate, large mini-batch sgd: Training imagenet in 1 hour. *arXiv preprint arXiv:1706.02677*, 2017. 2, 4, 7

[13] Chun-Hua Guo and Nicholas J Higham. A schur-newton method for the matrix p th root and its inverse. *SIAM Journal on Matrix Analysis and Applications*, 28(3):788–804, 2006. 6

[14] Tong He, Zhi Zhang, Hang Zhang, Zhongyue Zhang, Jun-yuan Xie, and Mu Li. Bag of tricks for image classification with convolutional neural networks. In *Proceedings of the IEEE/CVF Conference on Computer Vision and Pattern Recognition (CVPR)*, June 2019. 2, 4, 7

[15] Lei Huang, Xianglong Liu, Bo Lang, Adams Wei Yu, Yongliang Wang, and Bo Li. Orthogonal weight normalization: Solution to optimization over multiple dependent stiefel manifolds in deep neural networks. *arXiv preprint arXiv:1709.06079*, 2017. 4

[16] Lei Huang, Jie Qin, Yi Zhou, Fan Zhu, Li Liu, and Ling Shao. Normalization techniques in training dnns: Methodology, analysis and application. *arXiv preprint arXiv:2009.12836*, 2020. 2

[17] Lei Huang, Dawei Yang, Bo Lang, and Jia Deng. Decorrelated batch normalization. In *Proceedings of the IEEE Conference on Computer Vision and Pattern Recognition*, pages 791–800, 2018. 2, 4, 6, 14

[18] Lei Huang, Yi Zhou, Fan Zhu, Li Liu, and Ling Shao. Iterative normalization: Beyond standardization towards efficient whitening. In *Proceedings of the IEEE Conference on Computer Vision and Pattern Recognition*, pages 4874–4883, 2019. 2, 4, 6, 14

[19] David H Hubel and Torsten N Wiesel. Receptive fields, binocular interaction and functional architecture in the cat's visual cortex. *The Journal of physiology*, 160(1):106–154, 1962. 1, 5, 10

[20] Aapo Hyvriinen, Jarmo Hurri, and Patrick O. Hoyer. *Natural Image Statistics: A Probabilistic Approach to Early Computational Vision*. Springer Publishing Company, Incorporated, 1st edition, 2009. 5

[21] Sergey Ioffe and Christian Szegedy. Batch normalization: Accelerating deep network training by reducing internal covariate shift. *arXiv preprint arXiv:1502.03167*, 2015. 2, 3

[22] Diederik P Kingma and Jimmy Ba. Adam: A method for stochastic optimization. *arXiv preprint arXiv:1412.6980*, 2014. 2, 4

[23] Alex Krizhevsky. One weird trick for parallelizing convolutional neural networks. *arXiv preprint arXiv:1404.5997*, 2014. 2

[24] Hao Li, Pratik Chaudhari, Hao Yang, Michael Lam, Avinash Ravichandran, Rahul Bhotika, and Stefano Soatto. Rethinking the hyperparameters for fine-tuning, 2020. 12

[25] Hao Li, Zheng Xu, Gavin Taylor, and Tom Goldstein. Visualizing the loss landscape of neural nets. *CoRR*, abs/1712.09913, 2017. 2

[26] Tsung-Yi Lin, Michael Maire, Serge Belongie, James Hays, Pietro Perona, Deva Ramanan, Piotr Dollár, and C Lawrence Zitnick. Microsoft coco: Common objects in context. In *European conference on computer vision*, pages 740–755. Springer, 2014. 2

[27] James Martens. Deep learning via hessian-free optimization. 2010. 2

[28] James Martens and Roger B. Grosse. Optimizing neural networks with Kronecker-factored approximate curvature. *CoRR*, abs/1503.05671, 2015. 2, 3

[29] Jorge Nocedal and Stephen Wright. *Numerical optimization*. Springer Science & Business Media, 2006. 2

[30] Xingang Pan, Xiaohang Zhan, Jianping Shi, Xiaou Tang, and Ping Luo. Switchable whitening for deep representation learning. In *Proceedings of the IEEE/CVF International Conference on Computer Vision*, pages 1863–1871, 2019. 2, 4, 6, 14

[31] Chao Peng, Tete Xiao, Zeming Li, Yuning Jiang, Xiangyu Zhang, Kai Jia, Gang Yu, and Jian Sun. Megdet: A large mini-batch object detector. *CoRR*, abs/1711.07240, 2017. 1, 2, 4, 7

[32] Siyuan Qiao, Huiyu Wang, Chenxi Liu, Wei Shen, and Alan Yuille. Micro-batch training with batch-channel normalization and weight standardization, 2020. 2, 4

[33] Tim Salimans and Diederik P. Kingma. Weight normalization: A simple reparameterization to accelerate training of deep neural networks. *CoRR*, abs/1602.07868, 2016. 2

[34] Saurabh Singh and Shankar Krishnan. Filter response normalization layer: Eliminating batch dependence in the training of deep neural networks. In *Proceedings of the IEEE/CVF Conference on Computer Vision and Pattern Recognition*, pages 11237–11246, 2020. 1, 2, 3, 4, 11

[35] Samuel L. Smith, Pieter-Jan Kindermans, and Quoc V. Le. Don’t decay the learning rate, increase the batch size. In *International Conference on Learning Representations*, 2018. 7, 10

[36] Ilya Sutskever, James Martens, George Dahl, and Geoffrey Hinton. On the importance of initialization and momentum in deep learning. In *International conference on machine learning*, pages 1139–1147, 2013. 8

[37] Ashish Vaswani, Noam Shazeer, Niki Parmar, Jakob Uszkoreit, Llion Jones, Aidan N. Gomez, Łukasz Kaiser, and Illia Polosukhin. Attention is all you need, 2017. 13

[38] Tong Wang, Yousong Zhu, Chaoyang Zhao, Wei Zeng, Yaowei Wang, Jinqiao Wang, and Ming Tang. Large batch optimization for object detection: Training coco in 12 minutes. 2, 4, 7

[39] Yuxin Wu and Kaiming He. Group normalization. *CoRR*, abs/1803.08494, 2018. 1, 2, 3, 4, 7, 8, 11

[40] Junjie Yan, Ruosi Wan, Xiangyu Zhang, Wei Zhang, Yichen Wei, and Jian Sun. Towards stabilizing batch statistics in backward propagation of batch normalization. *arXiv preprint arXiv:2001.06838*, 2020. 6, 12

[41] Chengxi Ye, Matthew Evanusa, Hua He, Anton Mitrokhin, Tom Goldstein, James A. Yorke, Cornelia Fermüller, and Yiannis Aloimonos. Network deconvolution. In *International Conference on Learning Representations*, 2020. 1, 2, 4, 5, 6, 14

[42] Chengxi Ye, Anton Mitrokhin, Chethan Parameshwara, Cornelia Fermüller, James A. Yorke, and Yiannis Aloimonos. Unsupervised learning of dense optical flow and depth from sparse event data. *CoRR*, abs/1809.08625, 2018. 2, 6, 14

[43] Chengxi Ye, Yezhou Yang, Cornelia Fermüller, and Yiannis Aloimonos. On the importance of consistency in training deep neural networks. *CoRR*, abs/1708.00631, 2017. 2, 3, 6

[44] Hongwei Yong, Jianqiang Huang, Deyu Meng, Xiansheng Hua, and Lei Zhang. Momentum batch normalization for deep learning with small batch size. In *European Conference on Computer Vision*, pages 224–240. Springer, 2020. 6

[45] Yang You, Igor Gitman, and Boris Ginsburg. Scaling sgd batch size to 32k for imagenet training. 2017. 2, 4

[46] Matthew D Zeiler and Rob Fergus. Visualizing and understanding convolutional networks. In *European conference on computer vision*, pages 818–833. Springer, 2014. 1

A. Cat Receptive Fields

B. Further Discussion

We can compute the covariance matrix $Cov_1 = X'_1 X_1$ from the data matrix X_1 of feature channel 1 to remove the

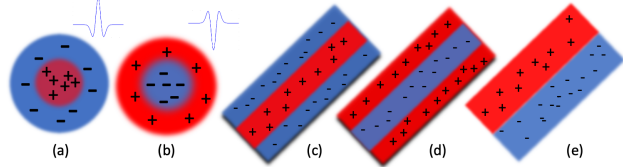


Figure 5. Receptive fields in the cat retina. Reproduced from [19], Fig. 2.

correlation in nearby pixels. For multiple channels we construct $X = [X_1, \dots, X_C]$ and compute a larger covariance matrix $Cov = X' X$. The diagonal blocks $X'_i X_i$ of this matrix measure the correlation of nearby pixels in each channel. The off-diagonal blocks $X'_i X_j$ measures the (pixel-wise) correlation across different channels (i and j). The transform we propose has a simple form for each sample: $z(x) = \Sigma^{-0.5}(s(x) - \mu)$, here $s(x)$ is a simple scaling for each sample. μ, Σ are computed from a batch.

Our formulation in Sec. 4 is based on the mathematical convolution. In most deep learning packages, the ‘convolution’ is implemented without flipping the kernel, and therefore, is in fact the ‘correlation’ operation. This misnaming does not affect the properties that we discuss throughout the paper.

B.1. Scale Invariance

We present our argument on scale invariance based on linear transforms without the bias term. Though the bias term can potentially mitigate the problem, it cannot introduce scale invariance. In classification problems, the softmax function introduces scale invariance to the logits. This is why we see smaller improvement from scale invariance compared to object detection.

B.2. GL(n)-Invariance

Here we present a global picture of $GL(n)$ -invariance. The ideal solution is to generate the global loss landscape with the whole dataset (Fig. 6(red)). Due to hardware limitations, training is conducted in minibatches. During training, different batches of data give rise to different loss landscapes (Fig. 6(green and blue)). These landscapes from sampled data generate noisy gradient directions that do not lead to the optimal solution for the whole dataset (Fig. 6(red)). Gradient descent follows these noisy gradients in an online fashion to update weights. Due to this approximation, it is beneficial to use learning rate decay or increase the batch size [35] towards the end of the training. However, using the running average covariance matrix to transform a batch of data yields poor performance. This wrong transform can result in a heavily curved loss landscape. Therefore, the covariance needs to be calculated from the same batch of data to avoid divergence. The evaluation, however, is based on the global loss landscape over

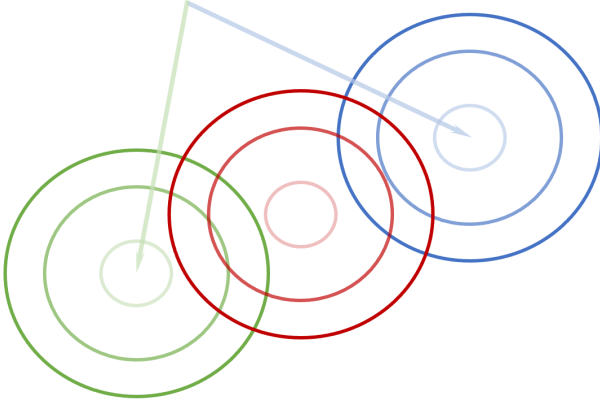


Figure 6. During the training, every minibatch has an individual loss landscape (visualized in green and blue). These loss landscapes are used during the training. During the testing, the global loss landscape (visualized in red) is used. This picture gives us intuition about the training/testing inconsistency and how issue should be properly addressed, as discussed in the text.

the whole dataset (Fig. 6(red)). The global transform can be achieved through the use of running average statistics. Methods that use global statistics such as the batch normalization are known to have this inconsistency in training and testing. The inconsistency can be alleviated by reducing the learning rate towards the end of the training or calculating the global statistics more accurately. One can also transform back to the original space (with the help of $Cov^{\frac{1}{2}}$) to eliminate the inconsistency. The methods that only utilize local statistics [5, 39, 34] to achieve consistency in training and testing in fact use a suboptimal geometry in the training and therefore have slower convergence.

C. Complexity Analysis

We derive the complexity of our proposed transform in a matrix multiplication layer $Y = (S \cdot X) \cdot (Cov^{-\frac{1}{2}} \cdot W)$. W is the weight matrix and has dimensions $Ch_{in} \times Ch_{out}$. $S \cdot X$ introduces scale invariance. Note that S is either diagonal or augmented with an extra column if we include bias. The complexity is $O(N \times Ch_{in})$, which is linear to the scale of X . We put the emphasis on the computation of $Cov^{-\frac{1}{2}} \cdot W$. We first assume X has been reshaped to $N \cdot \frac{Ch_{in}}{B} \times B$. The covariance matrix is calculated based on the reshaped X , and has a size of $B \times B$. The computation of the covariance matrix has complexity $O(B \cdot \frac{N \cdot Ch_{in}}{B} \cdot B) = O(N \cdot Ch_{in} \cdot B)$. Coupled inverse Newton-Schulz iterations (5-iterations) are therefore conducted on matrices of size $B \times B$. Solving for the inverse square root takes $O(B^3)$. Next we assume W has been reshaped from $Ch_{in} \times Ch_{out}$ to $B \times (\frac{Ch_{in} \cdot Ch_{out}}{B})$, weight transform $Cov^{-\frac{1}{2}} \cdot W$ is a simple matrix multiplication with complexity $O(B^2 \cdot \frac{Ch_{in} \cdot Ch_{out}}{B}) = O(B \cdot Ch_{in} \cdot Ch_{out})$.

<i>Kernel</i>	7	3	3	1	1
<i>Stride</i>	2	1	1	1	2
<i>Ch_{in}</i>	3	64	256	512	2048
<i>Ch_{out}</i>	64	64	256	128	1024
<i>H</i>	800	200	200	100	50
<i>W</i>	1333	333	333	166	83
$\frac{x}{\sigma_1}$	0.75	0.99	3.84	1.94	1.95
$\frac{x-\mu}{\sigma_2}$	1.81	2.39	9.38	4.74	4.73
Get X	0.72	0.93	6.22	2.81	2.93
$Cov = \frac{1}{N} X^t X$	1.43	0.7	2.75	1.36	1.4
$D = Cov^{-\frac{1}{2}}$	0	0.14	0.13	0.13	0.13
$D \cdot W$	0	0	0.02	0.02	0.84
<i>Conv</i>	30.16	3.4	30.56	7.31	46.6

Table 8. CPU runtime (in seconds) for a few representative settings in a Mask R-CNN network. The top rows in the first block show the layout in the network, the rows in the second block shows the runtime for two local normalization methods, the rows in the third block show the runtime for the $GL(n)$ -invariance. The last row shows the runtime of the convolution layer.

The overall complexity is $O(N \cdot Ch_{in} \cdot B + B^3 + B \cdot Ch_{in} \cdot Ch_{out}) = O((N \cdot Ch_{in} + B^2 + Ch_{in} \cdot Ch_{out}) \cdot B)$. This can be a small fraction of the cost of the matrix multiplication operation that has a complexity of $O(N \times Ch_{in} \times Ch_{out})$ if we use a small B . The simple derivation above can be easily generalize to the case of convolution and correlation layers, and note that N approximately equals to the number of pixels at each layer.

D. Runtime Analysis

Here we report the CPU time for a few representative layers in a Mask R-CNN network to verify the claim about the complexity of our proposed algorithm (Table 8). The batch size is set to 16, the subsampling stride is set to 5 to compute the covariance matrix, and timing is averaged over 10 batches. Note that the overall computation required for introducing the $GL(n)$ -invariance is comparable to introducing scale invariance and is usually a small fraction of the time taken by the convolution layer. Moreover, extracting the data matrix, which takes the most time, *shares the same computation as the underlying convolution*, and therefore would not be required with proper optimization. At this moment, this sharing mechanism is not supported in software packages. This lack of low-level optimization leads to extended wall time in our experiments.

E. Experiment Details

E.1. Image Classification

For the ImageNet classification experiments, we tested three weight decay levels (1e-4/5e-4/1e-3) and report the highest accuracy for both the synchronized batch normal-

	Model Zoo Baseline		ND++	
	AP_{bbox}	AP_{mask}	AP_{bbox}	AP_{mask}
Faster R-CNN R101-FPN	42		43.24	
Mask R-CNN R101-FPN	42.9	38.6	43.86	39.96
Mask R-CNN R50-FPN (scratch)	39.9	36.6	41.12	37.36

Table 9. Comparison with Detectron2 3x baselines found in the model zoo. For our R101 results, we increase the batch size by 3x instead of the training steps.

	AP bbox	AP mask
Frozen BN	NaN	NaN
GN	33.46	31.09
ND++	38.02	35.09

Table 10. Results of using an initial starting learning rate 1.0 to train a Mask R-CNN network.

ization baseline and ND++. We have also tested batch normalization without synchronization and find the synchronized version usually gives a better result; we therefore use it as the baseline. The baseline model achieves the reported accuracy with weight decay factors $1e-4/5e-4/5e-4$ respectively for VGG-11/Resnet-50/DenseNet-121. Correlated features create pathological regions that prevents the usage of large weight decay (Fig 2). With ND++, larger weight decay factors can be used and the optimal factors are $5e-4/1e-3/1e-3$. For DenseNet, the baseline model takes more GPU RAM than the machine can hold and the result with batch size 1024 is reported here to compare with our batch size 2048 result. Due to the latency of the customized implementation, the wall time of ND++ is longer but still acceptable. By using the large batch size, the number of calls to the slow functions is reduced and we finish the training in a shorter time compared to the original batch size of 256. With batch size 256, the baseline with SyncBN took 29 hours to train the ResNet-50. With batch size 2048, the complete version of ND++ finishes in the same time with superior accuracy. If remove scale invariance, ND++ finishes in 24 hours with a negligible drop in accuracy. At batch size 2048, ND++ without scale invariance takes 23/24/36 hours for VGG-11/ResNet-50/DenseNet-121 while the SyncBN baselines take 18/19/21 hours. Enforcing scale invariance slows training by 20% with little change in performance. The experiments are conducted on an AWS EC2 P3dn.24x instance. Note that the reported timing allows plenty of room for future improvements: besides sharing the extraction of the data matrix, layerwise standardization can be accelerated with sampling techniques.

E.2. Object Detection

For object detection, we report additionally results of training Mask R-CNN on Detectraon 2. We attach figures of training from scratch with different learning rates (Supp. Fig. 7) and fine-tuning with large batch sizes(Supp. Fig. 8). In most experiments we achieve impressive performance ND++ while using a learning rate of 0.1 and a momentum

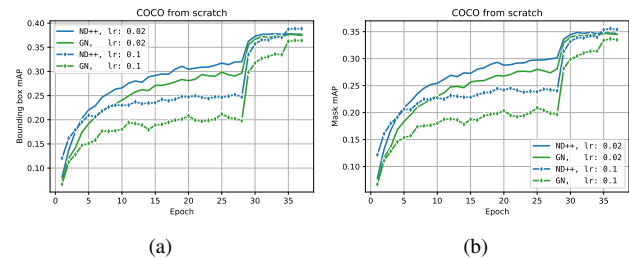


Figure 7. Bounding box and mask AP curves during validation when training the Mask R-CNN network from scratch. Note that with the more standard learning rate of 0.1, ND++ produces superior results compared to the GN baseline.

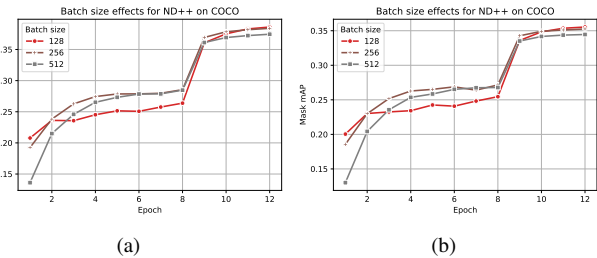


Figure 8. Bounding box and mask AP curves during validation when using large batch sizes to fine-tune the Mask R-CNN network.

of 0.9. This combination has an effective learning rate of 1.0 [24]. Our transformation can make better use of this optimal learning rate compared to existing methods. The partially corrected gradients with standardization have less optimal direction and less useful scale. Smaller learning rates need to be used to avoid divergence.

In this task, the lack of support to our customized implementation becomes more apparent due to the small training batch and layerwise standardization. In the MLPerf implementation, training and validating Mask R-CNN for 12 epochs takes 5 hours for the frozen batch normalization baseline, 6 hours for the group normalization baseline, can take more than 10 hours for ND++ using on an AWS EC2 P4d.24x instance with 8 GPUs. We notice that the seemingly simple layerwise standardization takes a significant amount of time. The runtime is 14 hours if we remove both scale and bias (Box AP 38.4), 11 hours if we remove just the scale (Box AP 38.3), and 9 hours if we do not apply scale invariance at all (Box AP 37.5). The wall time can be significantly reduced if we increase the batch size and reduce the number of function calls. At batch size 64, our slowest run takes 11 hours (3 hours faster), reaching Box AP 38.7, Mask AP 35.6, superior to a recent method that trains with 2x more steps [40]. Besides optimizing these operations through low-level changes to the software package, we can also use standardization layers in only a subset of the network. Our experimentation during development

Validation mIoU	
ND++	72.71
ND++ w/o scale inv.	72.69
ND++ w/o sync	69.82
BN	69.30

Table 11. Ablation studies for DeepLabv3 with a ResNet-50 backbone on the Cityscapes dataset. We train from scratch for each condition for 200 epochs.

indicates that applying standardization only in the RPN can maintain high-quality results. Here we report the numbers for the slow but universal design. For large batch experiments, we remove the warmup iterations and increase the weight decay factor for large batch sizes. For batch sizes of 128/256/512, the weight decay factors we use are 2.5e-4/5e-4/1e-3. We distribute the computation over 2/4/8 machines. For these experiments, slow inter-machine communication is the major bottleneck. We use the AWS Elastic Fiber Adaptor to speed up the inter-node communication *without changing the code*. These multi-machine experiments (including training and evaluation) finish in 7/5/4 hours respectively.

We also tested using an initial learning rate of 1.0 to train the Mask R-CNN network under different normalization techniques. We notice the training with Frozen Batch Normalization explodes early in the training. Group Normalization finishes with significantly worse results. ND++ ends up with competing results (Sup. Table 10).

E.3. Semantic Segmentation

For semantic segmentation, we use the 2975 images with fine annotations and report results on the validation split with 500 images. In all experiments, we perform standard data augmentation. We perform distributed training on 8-GPU machines for 200 epochs with a minibatch size of 3. We reduce the learning rate on a default polynomial schedule with exponent 0.9 and use a weight decay of 0.0001.

We see accelerated training and improved final performance on the validation set both when training from scratch and when fine-tuning with a pretrained backbone (Sup. Fig. 11 (a)). While the model equipped with ND++ layers takes approximately 30% longer per epoch to train, the accelerated training convergence more than makes up for the increased time per epoch (Fig. 11 (b)).

E.4. Training Transformer Models for Language Tasks

Here we also show promising results on training two Transformer models [37] for language tasks using the code from Fairseq [1]. We remove the Layer Normalization layers in the baseline Transformer model, and insert our modifications in the linear transform layers in the Transformer model. The original transformer models require warmup

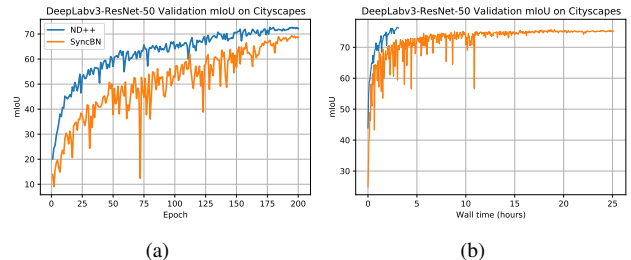


Figure 9. (a) Training on the Cityscapes dataset from scratch for 200 epochs. (b) Fine-tuning on the Cityscapes dataset using a backbone pretrained on Imagenet for 50 epochs with ND++ and 500 epochs with SyncBN. While each epoch takes longer with ND++ layers, the training convergence is still markedly faster in terms of wall time. Note that we use a learning rate of 0.1 for the ND++ model here.

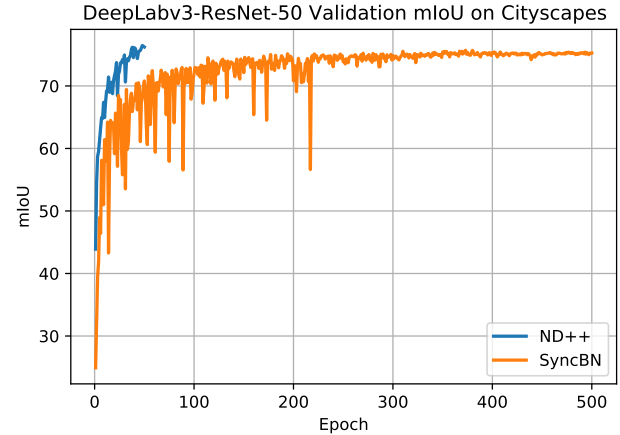


Figure 10. mIoU curves of DeepLabv3 with a ResNet-50 backbone trained on the Cityscapes dataset using ND++ and SyncBN. Here, we show that ND++ takes less than 50 epochs to achieve the same accuracy as SyncBN achieves in 500 epochs.

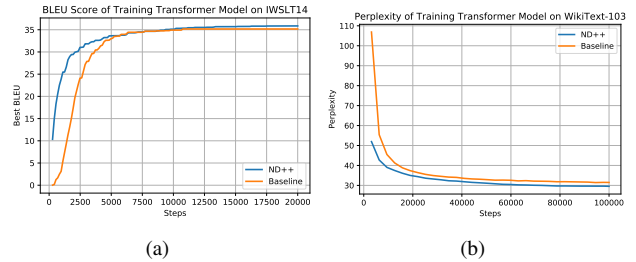


Figure 11. Training conducted using ND++ with a cosine learning rate decay versus the baseline with warmup and inverse square root decay. (a) BLEU score comparison on IWSLT14. (b) Perplexity comparison on WikiText-103.

iterations to warrant a successful training. After modification with ND++, we can start with a large learning rate and remove the warmup iterations. For the German to English translation task on the IWSLT14 dataset, the BLEU score

CIFAR-100		ImageNet		
ResNet-110	ResNet-50	IterNorm	SW	ND++
SW (160 epochs)	ND++ (80 epochs)	73.52	74.74	76.69
				77.66
				77.95

Table 12. Extra results on CIFAR-100 and ImageNet.

of ND++ after 20k iterations is 35.9 vs 35.2 of the baseline. For the language model training on WikiText-103, the Perplexity is reduced from 31.48 of the baseline model to 29.54. For these experiments the max token size is 4096 per GPU and we train on 8 Nvidia A100 GPUs. The baseline models are trained with the inverse square root learning decay after 4k warmup iterations. After modifying with ND++, we notice using a simple cosine learning rate decay as in vision tasks significantly accelerates the convergence.

F. Relation with Other Decorrelation Methods

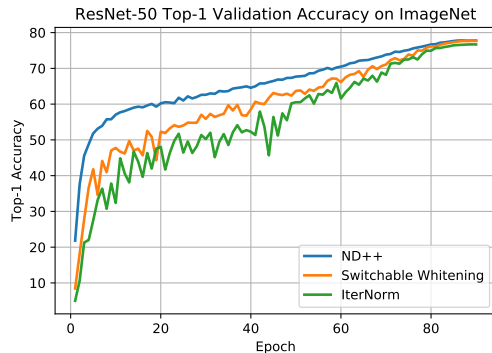


Figure 12. Top-1 validation accuracy curves of ResNet-50 when trained on ImageNet with ND++, Switchable Whitening(SW), IterNorm using batch size of 2048.

Here we highlight a few differences with recent whitening techniques [17, 18, 30]. Our deconvolution is a normalization in the frequency domain, and this is the optimal feature transform for convolution operation, while recent works are developed for non-convolutional operations. We follow the simple yet important mathematical justification to insert it before the weights, removing the redundancy and avoiding potential problems related with the extra parameters as in BatchNorm. Moreover, we avoid the computational cost of explicit decorrelation by fusing the decorrelation matrix with the weight matrix in the linear transform. Without this, the per-sample whitening could incur high computational cost. Due to this limitation, most recent works [17, 18, 30] have restricted the use of whitening to only a few layers of the network. And the coupled inverse newton iteration method we adopt, along with the Denman-Beavers iteration in [42] are stable to finite arithmetic while the vanilla Newton-Schulz method diverges if under certain conditions [41](Fig. 7).

We compare our results with IterNorm and Switchable Whitening(SW) in various settings according to their code availability. In all settings ND++ achieves faster and bet-

```
#PyTorch-like forward implementation for a linear layer
def forward_impl(input, weight, bias, groups=256, eps=1e-5):

    #1. scale-invariance
    input_norm=input.abs().mean(dim=-1,keepdim=True)
    input = input/ (input_norm + eps)

    #2. Calculate mu, cov, cov_isqrt
    X=input.reshape(-1, groups)
    X_mean = X.mean(0)
    XX_mean = X.t()@X.shape[0]
    Id = torch.eye(groups)
    cov= XX_mean- X_mean.unsqueeze(1) @X_mean.unsqueeze(0)+eps*Id
    cov_isqrt = isqrt_newton_schulz_autograd(cov)

    #3. S * X * D * W = (S * X) * (D * W)
    w = weight.view(-1, groups) @ cov_isqrt
    b = bias - (w @ (X_mean.unsqueeze(1))).view(weight.shape[0], -1).sum(1)
    w = w.view(weight.shape)
    return F.linear(input, w, b)
```

Figure 13. Reference modifications to a linear layer.

ter convergence than IterNorm and SW(Fig. 12). Interestingly, we found our simple design performs slightly better than the ensemble design of SW that incorporates multiple normalization/whitening techniques while using less computational space. This suggests that the ensemble design has potential for further improvement by including ND++ as a module (Table. 12). When training the ResNet-50 with learning rate 1.0 and no momentum on the ImageNet, ND++ achieves top accuracy of 77.66, versus SW of 76.85 and IterNorm of 76.57.

G. Source Code

We present a PyTorch-like code snippet showing our modifications to a linear layer.

Our full code release is available through:

<https://github.com/amazon-research/network-deconvolution-pp>

Our implementation of cross GPU synchronization borrows wisdom from the ‘diffdist’ repository:

<https://github.com/ag14774/diffdist>